Available online at www.sciencedirect.com
SCIENCE DIRECT®
Journal of Power Sources 131 (2004) 299–303
JOURNAL OF POWER SOURCES
www.elsevier.com/locate/jpowsour

Design of metal/oxide interfaces for the direct introduction of hydrocarbons into SOFCs

Teruhisa Horita*, Katsuhiko Yamaji, Tohru Kato, Natsuko Sakai, Harumi Yokokawa

National Institute of Advanced Industrial Science and Technology (AIST), Tsukuba central 5, Higashi 1-1-1, Tsukuba, Ibaraki 305-8565 Japan

Received 30 September 2003; accepted 25 October 2003

Abstract

Catalytic CH_4 decomposition and reactions of the reformed gases were examined on stripe-shaped Ni and Au electrodes on oxide substrates designed as optimum metal/oxide interfaces of SOFC anodes. The oxide substrates examined were Y_2O_3-stabilized ZrO_2 (YSZ) and Y_2O_3-doped CeO_2 (YDC). The isotope labeling technique has been applied to visualize the distribution of reacted species, such as H, C, and O. In mixtures of $CH_4 + D_2O + {}^{18}O_2$, the samples were annealed at 973 K and SIMS analysis was carried out on the quenched samples. On the YSZ substrates, Ni was active for CH_4 decomposition and carbon deposition, whereas the Au surface was inactive for the reaction. On the YDC substrates, the amounts of carbon deposited on the Ni surface were reduced due to their oxide ion conductivity and proton solubility. A possible reaction mechanism was considered for these metal/oxide interfaces.

Keywords: Hydrocarbon fuels; Direct introduction; Secondary ion mass spectrometry (SIMS); SOFC

1. Introduction

The direct introduction of hydrocarbons is one of the key issues relating to the operation of high performance solid oxide fuel cells (SOFCs). Direct introduction of hydrocarbons means reforming and power generation at the anode of SOFCs simultaneously. For reforming CH_4 in the SOFC cells, two possible ways can be considered; one is steam reforming and the other is partial oxidation. The present study focuses on steam reforming with small amounts of steam in the fuels (S/C $\leq$ 2) as follows:

$$CH_4 + H_2O = CO + 3H_2 \quad (1)$$

$$CO + H_2O = CO_2 + H_2 \quad (2)$$

At 1273 K, the steam reforming reaction proceeds very fast and a relatively high performance has been reported in SOFC stacks. When the operation temperature of SOFCs is reduced to lower than 1073 K, the steam/carbon ratio must be high enough (more than 2) to prevent carbon deposition. On the other hand, the amounts of steam should be as small as possible to maximize the efficiency of the SOFC system. Therefore, minimum steam partial pressure and electrochemical oxidation of CH_4 must be considered:

$$CH_4 + 4O^{2-} = CO_2 + 2H_2O + 8e^- \quad (3)$$

where O^{2-} is supplied from the cathode side of the electrolyte.

Recently, several authors have reported high performance SOFC anodes with hydrocarbon fuels under low steam or no steam conditions. Cu and Ni have been reported as active anode metals for the direct introduction of hydrocarbon fuels [1–3]. Also, alkali earth oxides [4], CeO_2-based oxides [5,6], TiO_2-based oxides [7], and $LaCrO_3$-based oxides [8] can be effective oxides for the direct introduction of CH_4 fuels. In real SOFC anodes, mixtures of metals and oxides ("cermets") have been adopted because of their high catalytic activity and structural stability. However, the porous anode cermet structure is very complicated as regards the effective factors for determining the catalytic activity of CH_4 decomposition and the reactions with the reformed gases.

In order to analyze the anode/electrolyte interfaces at the micron level, well-defined stripe-anode/electrolyte samples were prepared. The catalytic activity for CH_4 decomposition and the reaction with the reformed gases were investigated by the stable isotope gas labeling technique. Secondary ion mass spectrometry (SIMS) analysis was applied to visualize the distribution of labeled species in the quenched samples. In this report, we show the effects of metals and oxides on the reactions with CH_4 and reformed gases. As test electrodes, stripe-shaped Ni and Au are examined. As oxide substrates,

* Corresponding author. Tel.: +81-29-861-4542; fax: +81-29-861-4540.
E-mail address: t.horita@aist.go.jp (T. Horita).

0378-7753/$ – see front matter © 2004 Elsevier B.V. All rights reserved.
doi:10.1016/j.jpowsour.2003.10.018

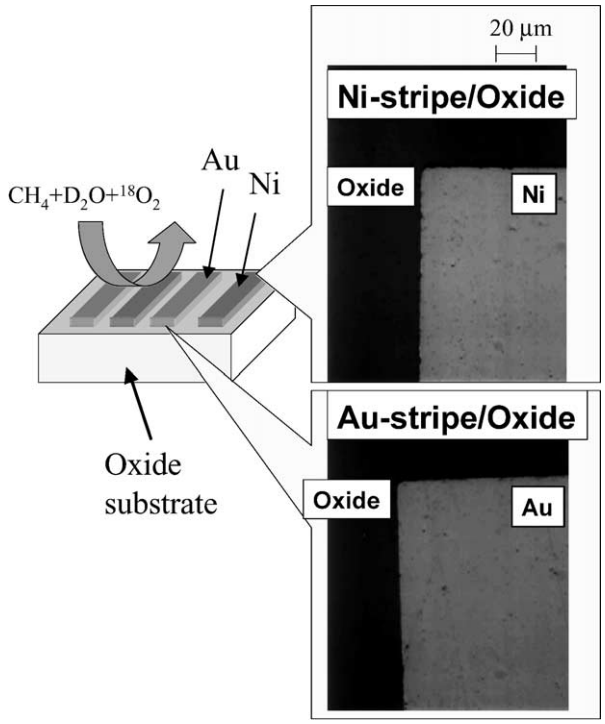

Fig. 1. Schematic diagram of isotope labeling (left) and optical microscope images (right) around the Ni-stripe and Au-stripe electrodes on the oxides.

yttria-stabilized zirconia (Y_2O_3-stabilized ZrO_2) and doped ceria (Y_2O_3-doped CeO_2) are examined. We compare the catalytic activity of different anode/oxide interfaces for designing high catalytic activity of CH_4 decomposition and reactions with the reformed gases.

2. Experiments

2.1. Samples

Fig. 1 shows microstructures of stripe anode/YSZ samples. Ni-stripe and Au-stripe electrodes were prepared by the RF-sputtering technique on sintered oxide substrates. We have chosen nickel (Ni) and gold (Au) as test anodes because Ni is a typical metal for porous anode materials [9–11] and Au is a typical standard electrode material for electrochemical analysis [12]. In Fig. 1, the brighter parts indicate the stripe electrode and the dark parts indicate the Y_2O_3-stabilized ZrO_2 (YSZ) substrate. As shown in the figures, the stripe anode/YSZ interfaces are clear and distinct boundaries without any voids between the anode and the electrolyte.

The oxide substrates examined were Y_2O_3-stabilized ZrO_2 ($Y_{0.15}Zr_{0.85}O_{1.925}$, YSZ) and Y_2O_3-doped CeO_2 ($Y_{0.2}Ce_{0.8}O_{1.9}$, YDC). The oxide substrates were sintered in air and polished with a diamond paste to obtain a flat surface. The thickness of the substrates was about 1 mm and the size of the substrates was 5 mm × 5 mm.

2.2. CH_4–H_2O treatment and isotope labeling

The gas mixture examined was CH_4, D_2O and $^{18}O_2$ to simulate steam reforming and direct introduction of CH_4 into SOFCs. The total gas pressure was 0.5 bar, and the partial pressures of the mixed gases were in the following ratio: $p(CH_4)/p(D_2O)/p(^{18}O_2) = 0.45\,\text{bar}/0.02\,\text{bar}/0.03\,\text{bar}$. D_2O and $^{18}O_2$ were used to label the movements of hydrogen and oxygen, respectively. The labeled gases were introduced at 973 K for 300 s. The thermodynamic equilibrium oxygen partial pressure is calculated to be around 10^{-25} bar, and the reformed gas composition is calculated as follows: $p(O_2) = 5.86 \times 10^{-25}$ bar, $p(H_2) = 4.32 \times 10^{-1}$ bar, $p(H_2O) = 8.82 \times 10^{-3}$ bar, $p(CO) = 3.23 \times 10^{-2}$ bar, $p(CO_2) = 1.06 \times 10^{-3}$ bar, $p(CH_4) = 2.58 \times 10^{-2}$ bar. This oxygen partial pressure is low enough to deposit carbon in the reactor tube. During the CH_4–H_2O treatment, the gas composition was checked with a mass monitor (RIGA-202, ULVAC Co.) by extracting small amounts of reaction gases. The measured $p(CO)/p(CO_2)$ ratio was about 100 (this value corresponded to an oxygen partial pressure of $p(O_2) = 2.1 \times 10^{-12}$ at 973 K), which indicated a far higher oxygen partial pressure in the exchanged gases. The deposited carbon can reduce the amount of CO in the gases. The gas mixture did not always reach equilibrium, even though a platinum mesh was used in the reactor tube as a sample holder.

2.3. SIMS analysis

After annealing in CH_4–D_2O–$^{18}O_2$ atmosphere, the samples were quenched to room temperature within 30 s. This technique enables us to observe a "frozen state" of labeled element distribution in the samples by secondary ion mass spectrometry (SIMS, CAMECA ims-5f, France) in its imaging mode. The primary ion beam was Cs^+ (acceleration voltage: 10 kV, primary beam current: less than 1 nA) and the distribution of negative secondary ions ($^2D^-$, $^{12}C^-$, $^{16}O^-$, $^{18}O^-$, $Ni^{16}O^-$, and $Zr^{16}O^-$) was measured in an area of 100 μm × 100 μm. After the SIMS analysis, the depths of the SIMS craters were measured by a surface profiler system (Dektak^3, Veeco/Sloan Technology, NY, USA).

3. Results and discussion

3.1. Effect of metals on the elemental distribution (comparison of Ni/YSZ and Au/YSZ interfaces by SIMS)

Fig. 2 shows SIMS images around the Ni-stripe/YSZ interfaces after the isotope labeling. The brighter parts in the images indicate the higher signal counts of each secondary ion. High concentrations of $^1H^-$ and $^{12}C^-$ are observed at the Ni parts, whereas low concentrations are observed at the YSZ parts. The concentration of $^2D^-$ is so low that we cannot observe the distribution clearly. For the distribution

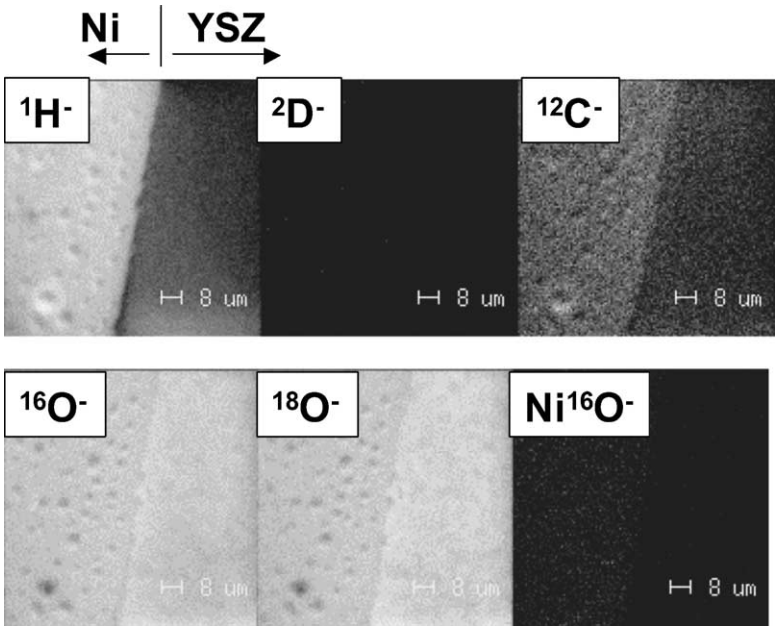

Fig. 2. SIMS scanning images around the Ni-stripe/YSZ interfaces.

of oxygen, the images of $^{16}O^{-}$ and $^{18}O^{-}$ show up with relatively high concentration at the Ni as well at the YSZ. This suggests that the activity for isotope oxygen exchange ($^{16}O/^{18}O$ exchange) is similar between the Ni and the YSZ surfaces. In order to analyze the SIMS image more quantitatively, a line analysis was examined around the Ni/YSZ interface (Fig. 3). The signals of $^{1}H^{-}$ and $^{12}C^{-}$ are high at the Ni part, whereas those of $^{16}O^{-}$ and $^{18}O^{-}$ are constant over all the surfaces. The signal counts of $^{1}H^{-}$ at the Ni part are about one order of magnitude higher than those at the YSZ. The signal counts of $^{12}C^{-}$ are about 700–800 cps at the Ni part, whereas they are 300–400 cps at the YSZ. Therefore, the signal counts of $^{12}C^{-}$ are about two times higher at the Ni than the YSZ. From the line analysis, the Ni surface is more active for the reaction with H and C than is the YSZ surface.

To compare the catalytic activity of metals, the Au/YSZ interfaces were analyzed with a similar method. Fig. 4 shows

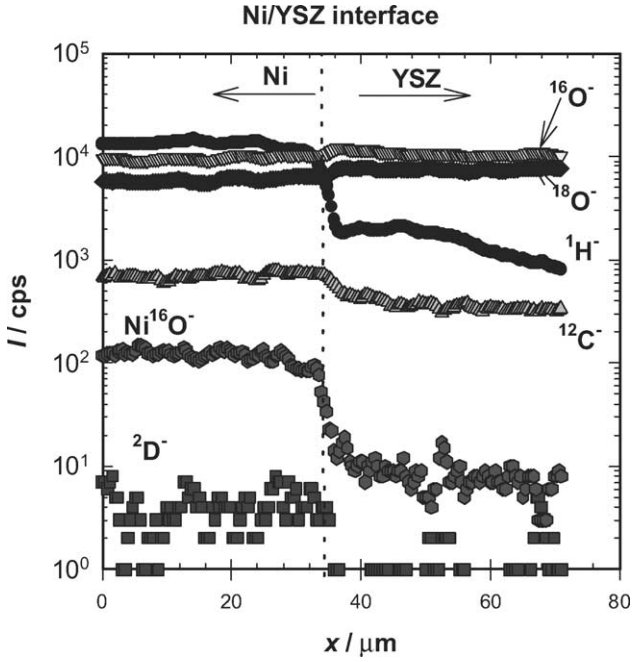

Fig. 3. Line analysis of SIMS images around the Ni-stripe/YSZ interfaces: (●), $^{1}H^{-}$; (■), $^{2}D^{-}$; (△), $^{12}C^{-}$; (◆), $^{16}O^{-}$; (▽), $^{18}O^{-}$; (⬢), $Ni^{16}O^{-}$.

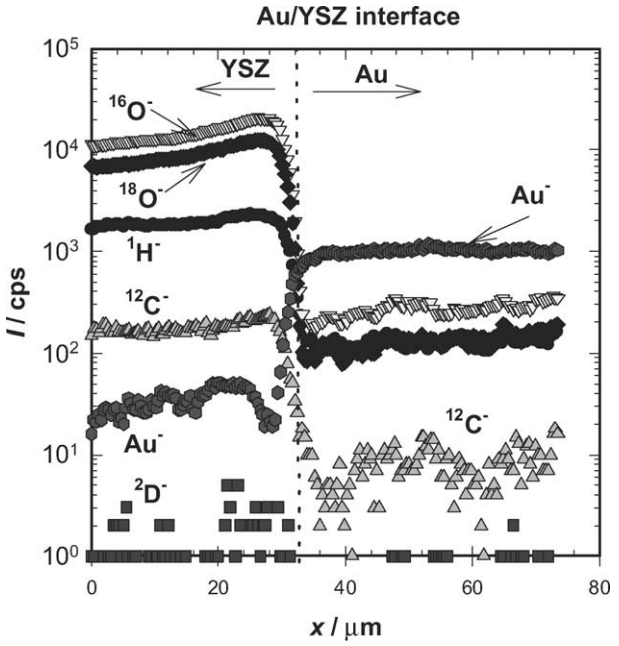

Fig. 4. Line analysis of SIMS images around the Au-stripe/YSZ interfaces: (●), $^{1}H^{-}$; (■), $^{2}D^{-}$; (△), $^{12}C^{-}$; (◆), $^{16}O^{-}$; (▽), $^{18}O^{-}$; (⬢), Au^{-}.

a line analysis around the Au-stripe/YSZ interfaces. High signal counts of $^{1}H^{-}$, $^{12}C^{-}$, $^{16}O^{-}$, and $^{18}O^{-}$ are observed at the YSZ parts whereas those signal counts are low at the Au part. Thus, the Au surface has low activity for CH_4 decomposition and/or the reaction with the reformed gases. The $^{16}O/^{18}O$ exchange reaction did not occur on the Au surface.

A significant difference of surface catalytic activity between the Ni and the Au was seen for the decomposition of CH_4: Ni was active for CH_4 decomposition and carbon deposition, whereas Au was inactive for these reactions. With respect to the form of carbon, it may be that Ni carbide or Ni carbonate can be formed on the surface, although we need more data to confirm this. Also, the distribution of oxygen (^{16}O and ^{18}O) was considerably different between Ni and Au. The Ni surface was oxidized and $^{16}O/^{18}O$ exchange occurred on the surface whereas almost no reaction took place on the Au surface. The metal/oxide interfaces are very clear in the SIMS images and the surface diffusion of oxygen or hydrogen was not detected in the SIMS imaging analysis. Thus the reaction zones at the metal/oxide interfaces are thought to be smaller than the resolution limits (may be less than 300 nm in this experimental condition).

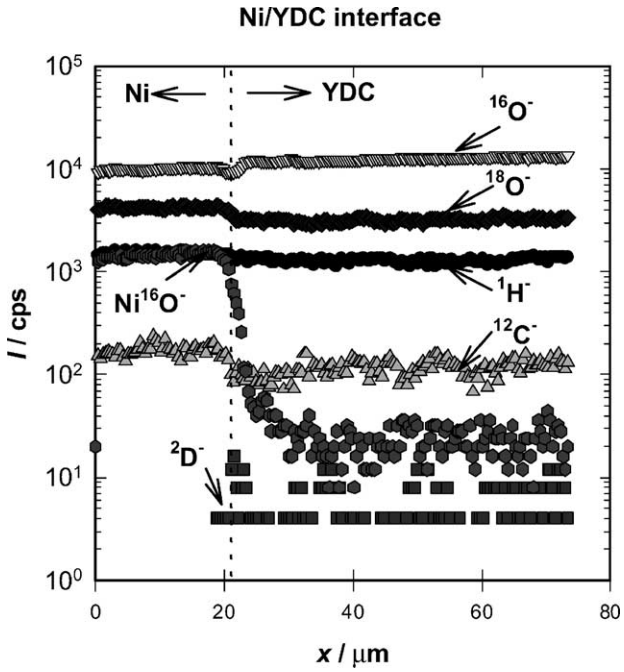

Fig. 5. Line analysis of SIMS images around the Ni-stripe/YDC interfaces: (●), $^{1}H^{-}$; (■), $^{2}D^{-}$; (▲), $^{12}C^{-}$; (◆), $^{16}O^{-}$; (▽), $^{18}O^{-}$; (◉), $Ni^{16}O^{-}$.

3.2. Effect of oxides on the elemental distribution (comparison of Ni/YSZ and Ni/YDC interfaces by SIMS)

Because the oxide substrates are oxide ion conductors, the diffusivity of oxide ions can affect the reactivity of gases around the metal/oxide interfaces. The oxygen vacancies at the oxide surfaces can be the reaction sites for oxygen incorporation. In addition, some hydrogen atoms can dissolve into CeO_2-based oxides as protons (H^+) [13,14]. Thus, oxide substrates can affect the distribution of H, C, and O around the metal/oxide interfaces. In this study, we compared the catalytic activity between YSZ and YDC for CH_4 decomposition and the reaction with H, C, and O. Fig. 5 shows SIMS image line analysis around the Ni-stripe/YDC interfaces after isotope labeling. The line analysis clearly indicates no significant increase of signal counts of $^{12}C^{-}$ and $^{1}H^{-}$ at the Ni surface, which is different from the Ni/YSZ interfaces (Fig. 3). This may be due to the surface diffusion of ions and electrons. It is also noted that the concentration of $^{18}O^{-}$ increases slightly at the Ni part. This suggests that the $^{16}O/^{18}O$ isotope exchange is promoted at the Ni surface. The nature of the surface of the YDC can affect the distribution of H, C, and O around the Ni/YDC interfaces.

3.3. Models of direct oxidation of CH_4 around the metal/oxide interfaces

From the SIMS images and line analyses, we can suggest the optimum metal/oxide interfaces for high catalytic activities of CH_4 decomposition and reaction with reformed gases. On the YSZ substrates, the Ni surface was active for CH_4 decomposition and carbon deposition, whereas the Au surface was inactive for carbon deposition. To reform CH_4 fuels, a high catalytic activity is needed for CH_4 decomposition. However, the decomposition of CH_4 will cause carbon deposition on the Ni surface. To reduce the amounts of carbon deposited on the Ni surface, a ceria-based oxide can be effective. On the YDC substrate, the amounts of carbon deposited were reduced on the Ni surface. Also, the YDC surface promotes the $^{16}O/^{18}O$ exchange on the Ni surface. This effect is schematically illustrated in Fig. 6. When water vapor adsorbs on the Ni surface, it is dissociated and hydrogen (H) is transported to the Ni/YDC interfaces. Since protons (H^+) can be dissolved in YDC, the transported H can be ionized as protons in YDC. The proton formed can react with O^{2-} to form H_2O, and this is evaporated as H_2O around the surface of YDC. This reaction may enhance the adsorption of water on the Ni surface, which eventually increases the concentration of oxygen on the Ni surface. With respect to the Ni/YSZ interfaces, the above reactions are limited to the gas/Ni/YSZ interfaces due to the low solubility of protons in YSZ. This reduces the emission of water vapor from the YSZ oxides. As a result, the amounts of oxygen on the Ni surface are reduced.

The present report only showed the results of catalytic activities of metal/oxide interfaces. In the near future, we will show the effects of oxide ion flow on the distribution of elements.

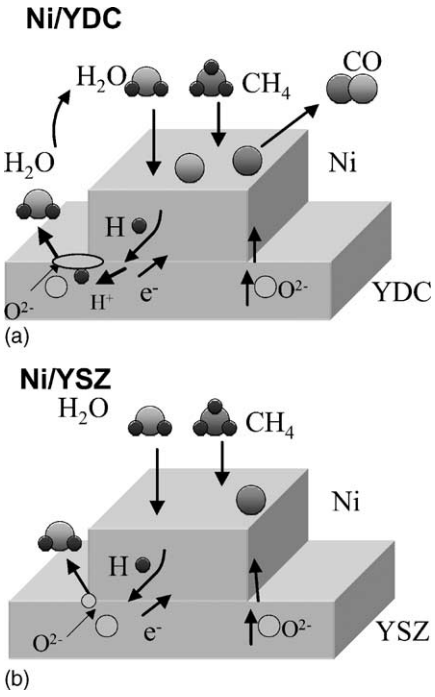

Fig. 6. Schematic diagram of CH_4 decomposition, and related gas reactions around the metal/oxide interfaces: (a) Ni/YDC, (b) Ni/YSZ.

4. Conclusions

At the stripe-shaped metal/oxide interfaces, catalytic activities for CH_4 decomposition and reaction of the reformed gases were compared. The isotope labeling technique has been applied to visualize the distribution of reacted species, such as H, C, and O. In mixtures of $CH_4 + D_2O + {}^{18}O_2$, the samples were annealed at 973 K and SIMS analysis was carried out on the quenched samples. On the YSZ substrate, Ni was active for CH_4 decomposition, whereas the Au was inactive for that reaction. The effect of oxide substrates on the CH_4 decomposition and the reaction with the reformed gases was compared between Y_2O_3-stabilized ZrO_2 (YSZ) and Y_2O_3-doped CeO_2 (YDC). On the YDC substrates, the amounts of carbon deposited on the Ni surface were reduced due to their proton solubility. A possible reaction mechanism was considered for these metal/oxide interfaces.

Acknowledgements

Part of this study was supported by Industrial Technology Research Grant Program in 2002–2003 from New Energy and Industrial Technology Development Organization (NEDO) of Japan. The corresponding author is grateful to the organization.

References

[1] H. Kim, S. Park, J.M. Vohs, R.J. Gorte, J. Electrochem. Soc. 148 (7) (2001) A693.
[2] H. Kim, C. Lu, W.L. Worrel, J.M. Vohs, R.J. Gorte, J. Electrochem. Soc. 149 (3) (2002) A247.
[3] G.C. Mather, D.P. Fagg, A. Ringuedé, Frade, Fuel Cells 1 (3/4) (2001) 233.
[4] T. Takeguchi, T. Yano, Y. Kani, R. Kikuchi, K. Eguchi, Solid Oxide Fuel Cells, vol. VIII, PV2003-17, The Electrochemical Society Inc., NJ, p. 704.
[5] O.A. Marina, C. Bagger, S. Primdahl, M. Mogensen, Solid State Ionics 123 (1999) 199.
[6] H. Uchida, S. Suzuki, M. Watanabe, Solid Oxide Fuel Cells, vol. VIII, PV2003-17, The Electrochemical Society Inc., NJ, p. 728.
[7] P. Holtappels, J. Bradley, J.T.S. Irvine, A. Kaier, M. Mogensen, J. Electrochem. Soc. 148 (8) (2001) A923.
[8] J. Sfeir, P.A. Buffat, P. Mökli, N. Xanthopoulos, R. Vasquez, H.J. Mathieu, J. Van herle, K.R. Thampi, J. Catalysis 202 (2001) 229.
[9] H. Itoh, T. Yamamoto, M. Mori, T. Horita, N. Sakai, H. Yokokawa, M. Dokiya, J. Electrochem. Soc. 144 (1997) 641.
[10] Y. Jiang, A.V. Virkar, J. Electrochem. Soc. 148 (7) (2001) A706.
[11] S.P. Jiang, Y. Duan, J.G. Love, J. Electrochem. Soc. 149 (9) (2002) A1175.
[12] B.A. van Hassel, B.A. Boukamp, A.J. Burggraaf, Solid State Ionics 48 (1991) 155.
[13] N. Sakai, K. Yamaji, T. Horita, H. Yokokawa, Y. Hirata, S. Sameshima, Y. Nigara, J. Mizusaki, Solid State Ionics 125 (1999) 325.
[14] N. Sakai, K. Yamaji, T. Horita, Y.P. Xiong, H. Kishimoto, H. Yokokawa, J. Electrochem. Soc. 150 (2003) A689.